Electronic Supplementary Information for

Significant Gas Uptake Enhancement by Post-Exchange of Zinc(II) with Copper(II) within a Metal-Organic Framework

Xiao-Jun Wang,[a] Pei-Zhou Li,[a] Lei Liu,[a] Quan Zhang,[a] Parijat Borah,[a] Jinye Daniel Wong,[a] Xiu Xiang Chan,[a] Ganguly Rakesh,[a] Yongxin Li[a] and Yanli Zhao*,[a,b]

[a] *Division of Chemistry and Biological Chemistry, School of Physical and Mathematical Sciences, Nanyang Technological University, 21 Nanyang Link, Singapore 637371*

[b] *School of Materials Science and Engineering, Nanyang Technological University, 50 Nanyang Avenue, Singapore 639798*

To whom correspondence should be addressed

Professor **Yanli Zhao**
Division of Chemistry and Biological Chemistry
School of Physical and Mathematical Sciences
Nanyang Technological University
21 Nanyang Link
Singapore 637371
E-mail: zhaoyanli@ntu.edu.sg
Phone: +65-63168792

General method and materials

All chemicals are commercially available and were used as received unless specifically mentioned. Dimethyl 5-azidoisophthalate (**3**)[S1] and dimethyl 5-ethynylisophthalate (**4**)[S2] were prepared according to the literature procedures. IR spectra were recorded as KBr-pellet on a Perkin-Elmer 1760X FT-IR spectrometer. NMR spectra were taken on either a Bruker AV 300 or a Bruker AV400 at room temperature. ESI-MS experiments were carried out on a ThermoFinnigan LCQ Fleet MS. Elemental analyses (C, H, and N) were obtained from EuroVector Euro EA Elemental Analyzer. Thermogravimetric analysis (TGA) was carried out on a TGA-Q500 thermoanalyzer with a heating rate of 5 °C/min under nitrogen atmosphere. The powder X-ray diffraction (PXRD) measurements were taken on a Bruker D8 diffractometer using Cu-K_α radiation (λ = 1.5418 Å) at room temperature. The metal ion concentrations were analyzed by using Thermo Fischer iCAP 6000 inductively coupled plasma optical emission (ICP-OES) spectrometer.

Synthesis

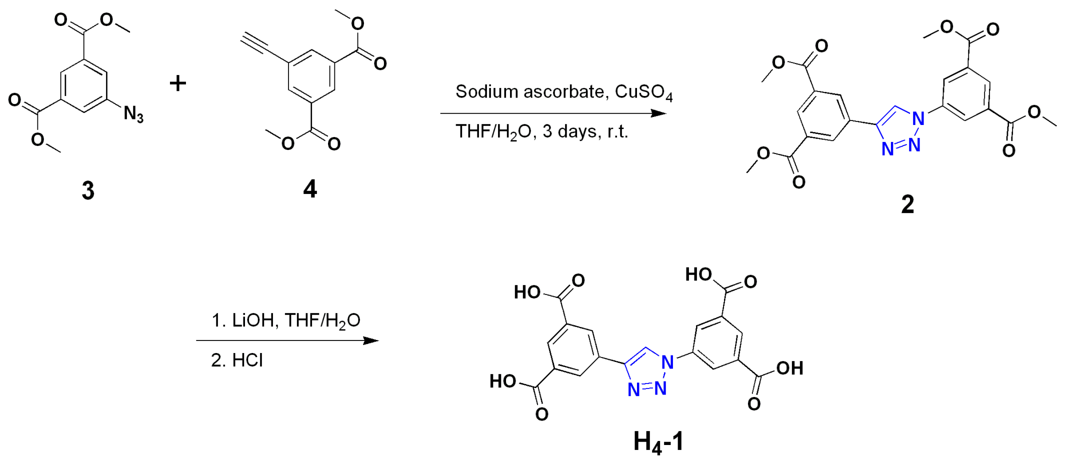

Scheme S1. Synthetic route for the preparation of **H_4-1**.

Tetramethyl 5,5'-(1*H*-1,2,3-triazole-1,4-diyl)diisophthalate (2). Dimethyl 5-azidoisophthalate (**3**, 0.24 g, 1.10 mmol) and dimethyl 5-ethynylisophthalate (**4**, 0.26 g, 1.10 mmol) were added into a mixture of THF/H_2O (50 mL/20 mL), and stirred at room temperature under Ar for 3 days. Then, the mixture was poured into water (50 mL) and extracted with CH_2Cl_2 (100 mL × 2). The combined organic layers were dried over Na_2SO_4 and the solvent was evaporated under vacuum. The crude product was purified by silica gel flash column chromatography (CH_2Cl_2/CH_3OH, 100/1) to give **2** as a white solid (0.46 g, 1.01 mmol, yield: 87%). ^{1}H NMR (300 MHz, $CDCl_3$) δ 8.79-8.78 (m, 3H), 8.70-8.69 (m, 3H), 8.49 (s, 1H), 4.03 (s, 6H), 4.00 (s, 6H). ^{13}C NMR (101 MHz, $CDCl_3$) δ 166.0, 165.0, 147.3, 137.3, 132.7, 131.6, 130.9, 130.8, 130.6, 125.1, 118.5, 53.1, 52.7. ESI-MS: *m/z* calcd for $C_{22}H_{19}N_3O_8$: 453.4, found: 454.2 $[M+H]^+$.

5,5'-(1*H*-1,2,3-triazole-1,4-diyl)diisophthalic acid (H_4-1). The ester **2** (0.56 g, 1.24 mmol) was hydrolyzed with excess LiOH (0.51 g, 21.3 mmol) in the mixture of THF (60 mL) and H_2O (30 mL) at room temperature overnight. Then, H_2O (50 mL) was added into the above solution and washed by Et_2O (100 mL × 2). The aqueous layer was acidified with HCl to pH = 1. The solid was collected by filtration, rinsed several times with distilled water, and dried to give **H_4-1** (0.48 g, 1.21 mmol, yield: 98%). ^{1}H NMR (300 MHz, DMSO) δ 13.59 (br, 4H), 9.96 (s, 1H), 8.77 (dd, *J* = 4.8, 1.4 Hz, 4H), 8.54 (t, *J* = 1.4 Hz, 1H), 8.47 (t, *J* = 1.5 Hz, 1H). ^{13}C NMR (101 MHz, DMSO) δ 166.4, 165.7, 146.1, 137.1, 133.3, 132.2, 131.1, 130.0, 129.5, 129.4, 123.8, 121.0. ESI-MS: *m/z* calcd for $C_{18}H_{11}N_3O_8$: 397.3, found: 398.2 $[M+H]^+$.

NTU-101-Zn. H_4-1 (40 mg, 0.10 mmol) and $Zn(NO_3)_2 \cdot 6H_2O$ (65 mg, 0.22 mmol) were dissolved in *N*,*N*-dimethylformamide (DMF, 12 mL). The solution was placed in a tightly capped 20 mL vial and heated at 75°C in an oven for 3 days. The colorless block crystals were collected after cooling down to room temperature. These crystals are insoluble in water and common organic solvents such as MeOH, EtOH, MeCN, chloroform, acetone, toluene, DMF, and DMSO. The crystals were washed by fresh DMF for 3 times and dried under vacuum. The obtained crystals were subjected to elemental analysis and TGA analysis in order to estimate the empirical formula as $Zn_2(\mathbf{1})(DMF)_3 \cdot DMF \cdot 3H_2O$ (25.6 mg, yield: 26% based on **H_4-1**). Elemental analysis calcd (%) for $C_{30}H_{41}N_7O_{15}Zn_2$: C 41.39, H 4.75, N 11.26; found: C 41.42, H 4.79, N 11.23. IR (KBr) (cm^{-1}): 1635(s), 1589(m), 1438(w), 1370(s), 1106(m), 1063(m), 777(m), 724(w), 667(w).

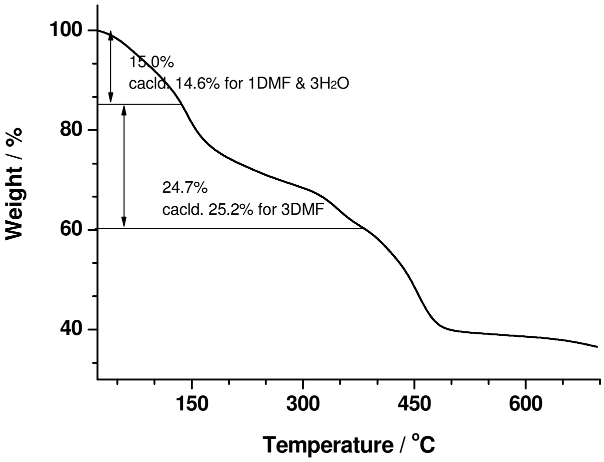

Fig. S1. TG curve of **NTU-101-Zn**.

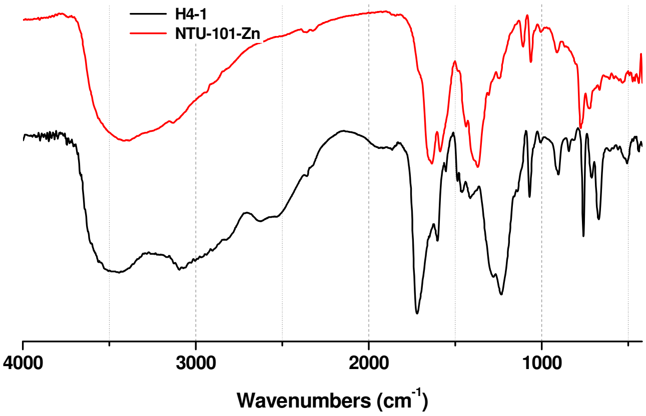

Fig. S2. FT-IR spectra of **H_4-1** and as-synthesized **NTU-101-Zn**.

Metal-ion exchange of NTU-101-Zn.[S3]

The as-synthesized crystals of **NTU-101-Zn** (around 50 mg) were initially washed by fresh DMF at least three times, and then added into a solution of $Cu(NO_3)_2$ (0.1 M, 15 mL) in DMF without stirring at room temperature for 3 weeks. The color of these crystals gradually changed from colorless to blue. During this period, the solution was replaced with fresh $Cu(NO_3)_2$ solution twice. After decanting the solvent, the cation-exchanged crystals (**NTU-101-Cu**) were washed thoroughly with DMF and suspended in fresh DMF at room temperature for one week in order to remove the excess metal ions from the channels of the framework, during which time the DMF was replaced three times, and then dried under vacuum. ICP analysis indicates that ~80% of Zn(II) was replaced by Cu(II) and no significant variation was observed with further extension of exchange time. The elemental analysis and TGA analysis were carried out to estimate the empirical formula of **NTU-101-Cu** as $Cu_{1.6}Zn_{0.4}(\mathbf{1})(DMF)_3\cdot 3DMF\cdot 7H_2O$. Elemental analysis calcd (%) for $C_{36}H_{63}N_9O_{21}Cu_{1.6}Zn_{0.4}$: C 39.85, H 5.85, N 11.62; found: C 39.92, H 5.83, N 11.02. IR (KBr) (cm^{-1}): 1658(s), 1586(m), 1438(w), 1371(s), 1103(m), 1062(m), 770(m), 727(w), 663(w).

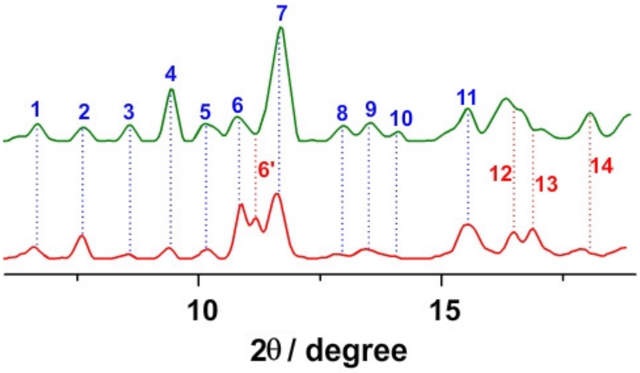

Fig. S3. Zoomed-in PXRD patterns of **NTU-101-Zn** (bottom) and **NTU-101-Cu** (top). The positions of main peaks (1-11) between the patterns well match by each other. The peak (6') in **NTU-101-Cu** may be merged into peaks (6 or 7). The small shifts of the peaks (12, 13, and 14) are probably caused by the little distortion of the framework as well as the fact that Cu(II) and Zn(II) are different elements.

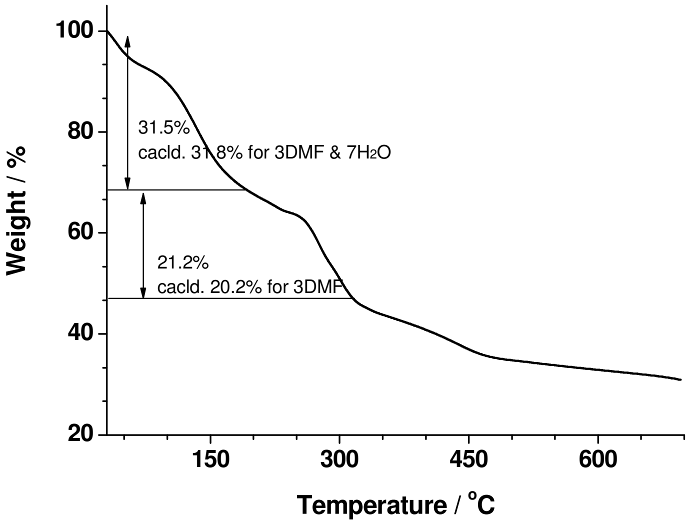

Fig. S4. TG curve of **NTU-101-Cu**.

The metal ion exchange of **NTU-101-Zn** by other divalent metal ions, such as Ni^{2+} and Co^{2+}, was conducted similarly in order to investigate the selectivity of metal ions. ICP analysis shows that there were 3.4% of Ni^{2+} (metal percentage) and 5.8% of Co^{2+} (metal percentage) in the corresponding metal-ion exchanged samples, indicating that the metal ion exchange of **NTU-101-Zn** is selective towards Cu^{2+} over Ni^{2+} and Co^{2+}.

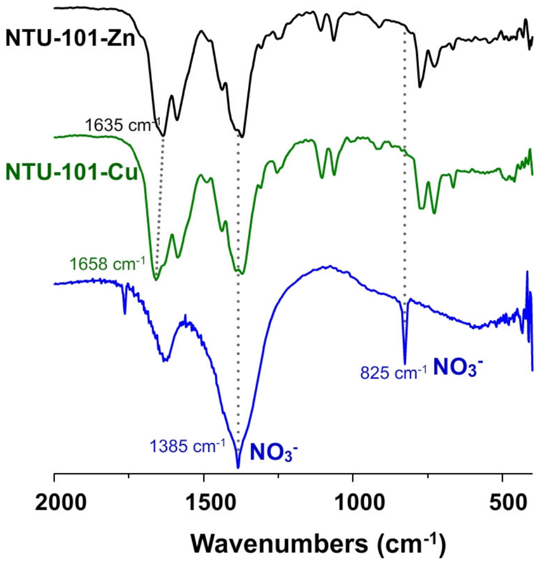

Fig. S5. FT-IR spectra of **NTU-101-Zn**, **NTU-101-Cu**, and NO_3^-.

The absence of NO_3^- stretching bands at 1385 and 825 cm^{-1} in the FT-IR spectrum of **NTU-101-Cu** indicates that no Cu^{2+} ions were absorbed in the pores of framework and/or coordinated with the triazole moiety. A similar IR spectrum to the parent **NTU-101-Zn** and the band shift from 1635 to 1658 cm^{-1} in **NTU-101-Cu** demonstrate that both of MOFs share a similar framework.

In addition, other Cu salts with different anions, including $Cu(CF_3SO_3)_2$, $CuSO_4$, $Cu(ClO_4)_2$, and $CuCl_2$, were used to carry out the metal ion exchange in **NTU-101-Zn** for one week, respectively. The ICP analysis for the exchanged samples indicated that the Zn ions in the parent MOF could be exchanged with Cu ions, although the Cu(II) contents in the exchanged samples are different (the contents of Cu(II) in the exchanged samples: $Cu(CF_3SO_3)_2$: Cu% = 20%; $CuSO_4$: Cu% = 69%; $Cu(ClO_4)_2$: Cu% = 57%; $CuCl_2$: Cu% = 93%). The Powder XRD and FT-IR studies demonstrated that the exchanged samples share similar framework with the parent MOF (Fig. S6-S8).

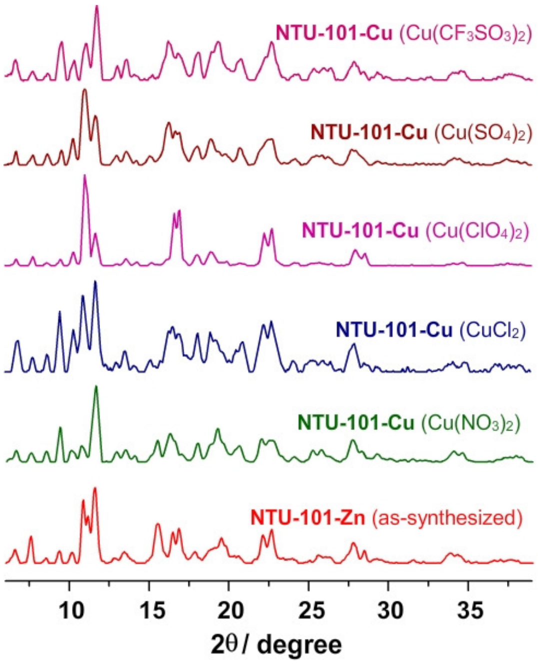

Fig. S6. Powder XRD patterns of **NTU-101-Cu** prepared with different Cu salts. The similar Powder XRD patterns suggest that the exchanged MOFs share the similar framework with the parent MOF.

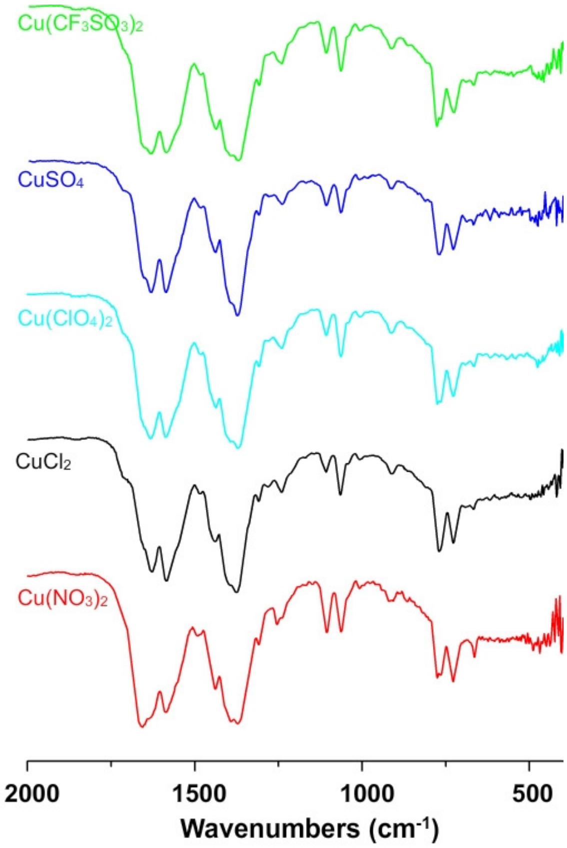

Fig. S7. FT-IR spectra of **NTU-101-Cu** prepared with different Cu salts. The similar FT-IR spectra suggest that the exchanged MOFs share similar framework with the parent MOF.

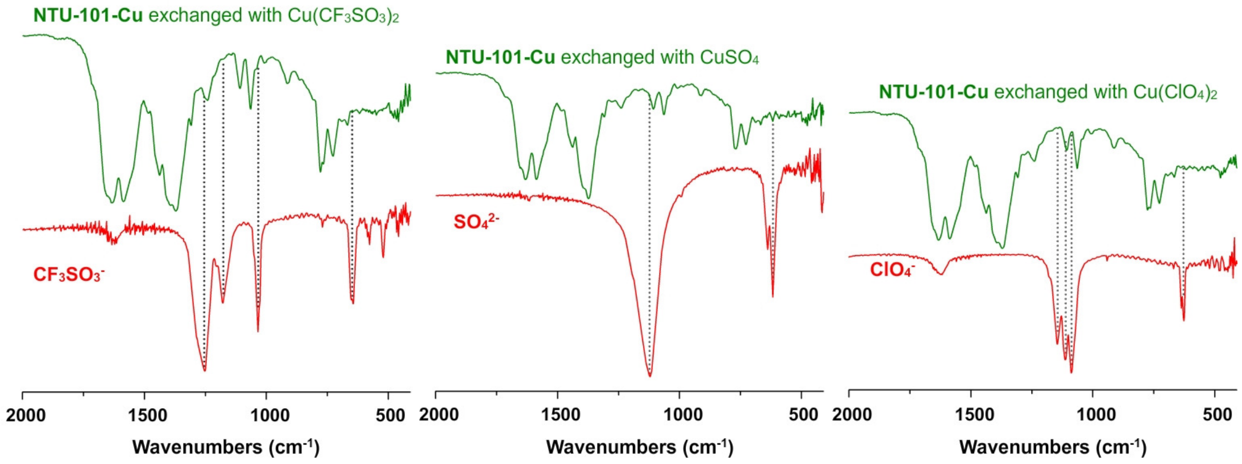

Fig. S8. FT-IR spectra of different Cu salts and **NTU-101-Cu** prepared from these Cu salts. The absence of typical stretching bands of corresponding anions demonstrates that the triazole rings in **NTU-101-Cu** are coordinatively free.

Kinetic studies of Cu(II)-ion exchange process

Since the as-synthesized crystals present quite different sizes, a ground sample was employed to study the kinetic process of Cu(II) ion exchange as shown below.

Ground crystals of **NTU-101-Zn** were immersed in a solution of $Cu(NO_3)_2$ (0.1 M, 20 mL) in DMF. A small amount of sample was taken out under regular intervals, washed thoroughly with DMF, and then kept in DMF for one week (DMF was replaced three times to remove the excess Cu^{2+}) followed by drying the sample under vacuum before subjected to the ICP analysis.

The Cu(II) ion exchange process using the ground sample was rapid and facile. Almost 80% of Zn(II) from the framework was replaced by Cu(II) within 6 h and no significant change was detected in the following days, as shown in Figure S9. For freshly prepared crystals, it will take approximately 2 weeks to achieve a similar amount of Zn(II) exchange. The metal ion exchange from Cu(II) back to Zn(II) is irreversible, even in a more concentrated DMF solution containing $Zn(NO_3)_2$ (0.3 M) and under long exchange time (1 month), evidenced by no crystal color change and no obvious variation of n_{Cu}/n_{Zn} ratio based on the ICP results before and after the exchange.

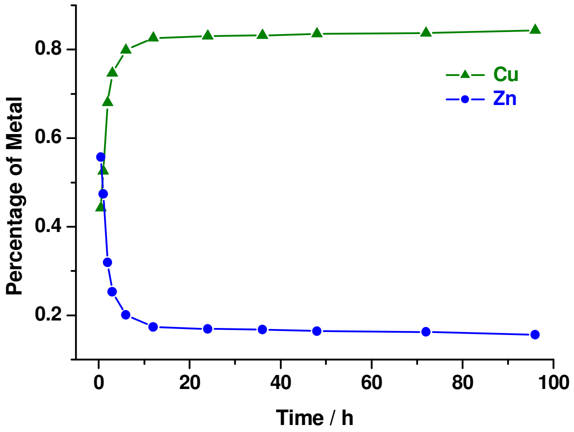

Fig. S9. Kinetic profile of the metal-ion exchange of Zn(II) by Cu(II) in **NTU-101-Zn**.

Attempted direct synthesis of ***NTU-101-Cu***

H_4-1 (40 mg, 0.10 mmol) and $Cu(NO_3)_2 \cdot 2.5H_2O$ (48 mg, 0.21 mmol) were dissolved in *N*,*N*-dimethylformamide (DMF, 12 mL). The solution was placed in a tightly capped 20 mL vial and heated at 75°C in an oven for 3 days. Light blue powder was obtained at the bottom of the vial, and the single crystal determination was unsuccessful under the current conditions. The powder XRD analysis indicates that the prepared sample has different phases from **NTU-101-Cu**, suggesting that the Cu(II)-ion exchanged MOF cannot be synthesized directly.

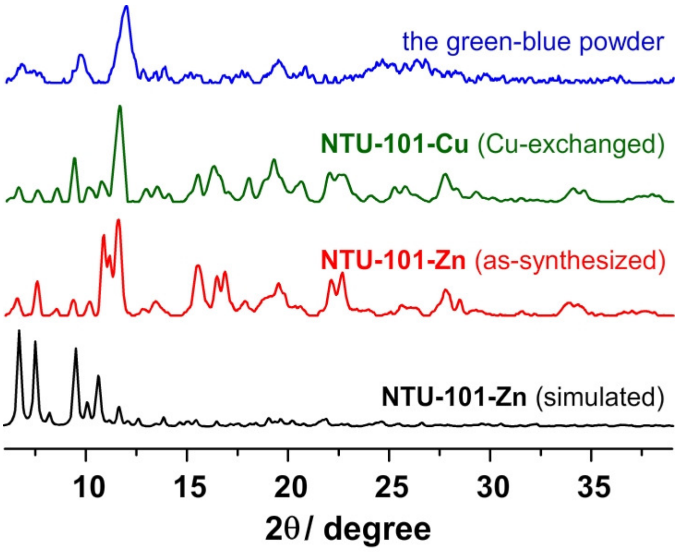

Fig. S10. Powder XRD patterns of **NTU-101-Cu** and the directly synthesized Cu(II)-containing materials.

Gas sorption

Low-pressure gas sorption measurements were performed by using Quantachrome Instruments Autosorb-iQ (Boynton Beach, Florida USA) with the extra-high pure gases. The as-synthesized **NTU-101-Zn** and **NTU-101-Cu** crystals were immersed in CH_2Cl_2 (30 mL) for 1 day, during which time CH_2Cl_2 was replaced three times. The samples were then moved into a sample cell and dried under vacuum at 60 °C by using the "outgasser" function for 12 h before the measurement. The Brunauer–Emmett–Teller (BET) surface area, pore size distribution, and total pore volume were calculated from the N_2 sorption isotherms at 77 K based on Non-Local Density Functional Theory (NL-DFT) model in the Quantachrome ASiQwin 2.01 software package. The isosteric heat of adsorption (Q_{st}) for CO_2, defined as

$$Q_{st} = RT^2\left(\frac{\partial \ln p}{\partial T}\right)_q \quad \text{(Clausius-Clapeyron equation)}$$

was determined by using the CO_2 adsorption isotherms at 273 and 298 K (ASiQwin 2.01).

X-ray crystallography.

The single crystal **NTU-101-Zn** for X-ray analysis was picked up under a microscope from a freshly synthesized solution and then mounted immediately. The diffraction data were collected at 103 K using graphite-monochromated Mo-*Kα* radiation (λ = 0.71073 Å) on a Bruker CCD APEXII diffractometer. The collected frames were processed with the software SAINT[S4]. The data were corrected for absorption by using the SADABS program[S5]. The structure was solved by the direct methods and refined by full-matrix least-squares analyses on F^2 (SHELXTL-97[S6]). There are a lot of disorders for the DMF molecules coordinated to the metal centers. These disorders were treated as multiple components using constrained geometry. The solvent molecules in **NTU-101-Zn** are highly disordered and cannot be modeled (except two solvent DMF molecules), thus the SQUEEZE routine of PLATON was applied to remove the contributions of the solvent molecules to the scattering. Crystallographic data for **NTU-101-Zn** is summarized in Table S1. CCDC 890896 contains the supplementary crystallographic data for **NTU-101-Zn**. These data can be obtained free of charge from The Cambridge Crystallographic Data Centre via www.ccdc.cam.ac.uk/data_request/cif.

Table S1. Crystal data and structure refinement for **NTU-101-Zn**.

Empirical formula	$C_{117}H_{133}N_{27}O_{47}Zn_8$	
Formula weight	3192.62	
Temperature	103(2) K	
Wavelength	0.71073 Å	
Crystal system	Orthorhombic	
Space group	*Pccn*	
Unit cell dimensions	a = 26.4360(4) Å	α = 90°.
	b = 26.1150(4) Å	β = 90°.
	c = 26.3473(4) Å	γ = 90°.
Volume	18189.5(5) Å^3	
Z	4	
Density (calculated)	1.166 Mg/m^3	
Absorption coefficient	1.130 mm^{-1}	
F(000)	8320	
Crystal size	0.34 x 0.28 x 0.08 mm^3	
Theta range for data collection	1.73 to 30.11°.	
Index ranges	-37<=h<=31, -36<=k<=36, -37<=l<=33	
Reflections collected	180525	
Independent reflections	26771 [R(int) = 0.0636]	
Completeness to theta = 30.11°	99.8 %	
Absorption correction	Semi-empirical from equivalents	
Max. and min. transmission	0.9151 and 0.7000	
Refinement method	Full-matrix least-squares on F^2	
Data / restraints / parameters	26771 / 2145 / 1283	
Goodness-of-fit on F^2	1.034	
Final R indices [I>2sigma(I)]	R_1 = 0.0633, wR_2 = 0.1905	
R indices (all data)	R_1 = 0.0957, wR_2 = 0.2056	
Largest diff. peak and hole	2.000 and -0.969 e.Å	

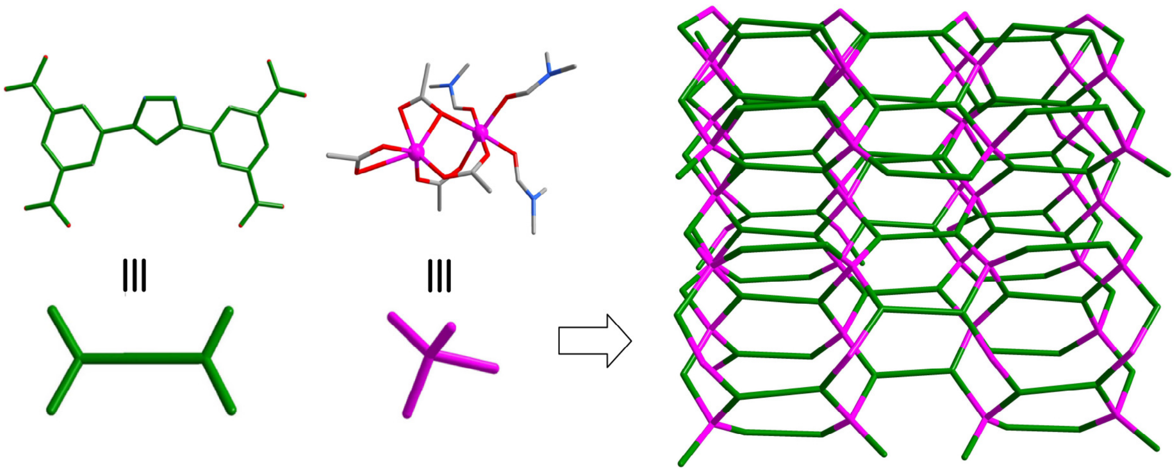

Fig. S11. The simplified view of PtS-type network of **NTU-101-Zn**. The [$Zn_2(CO_2)_4(DMF)_3$] secondary building unit can be viewed as a 4-connected node (purple, tetrahedral SBU), and the organic linker **1** that coordinates to four [$Zn_2(CO_2)_4(DMF)_3$] units acts as a 4-connected node (green).

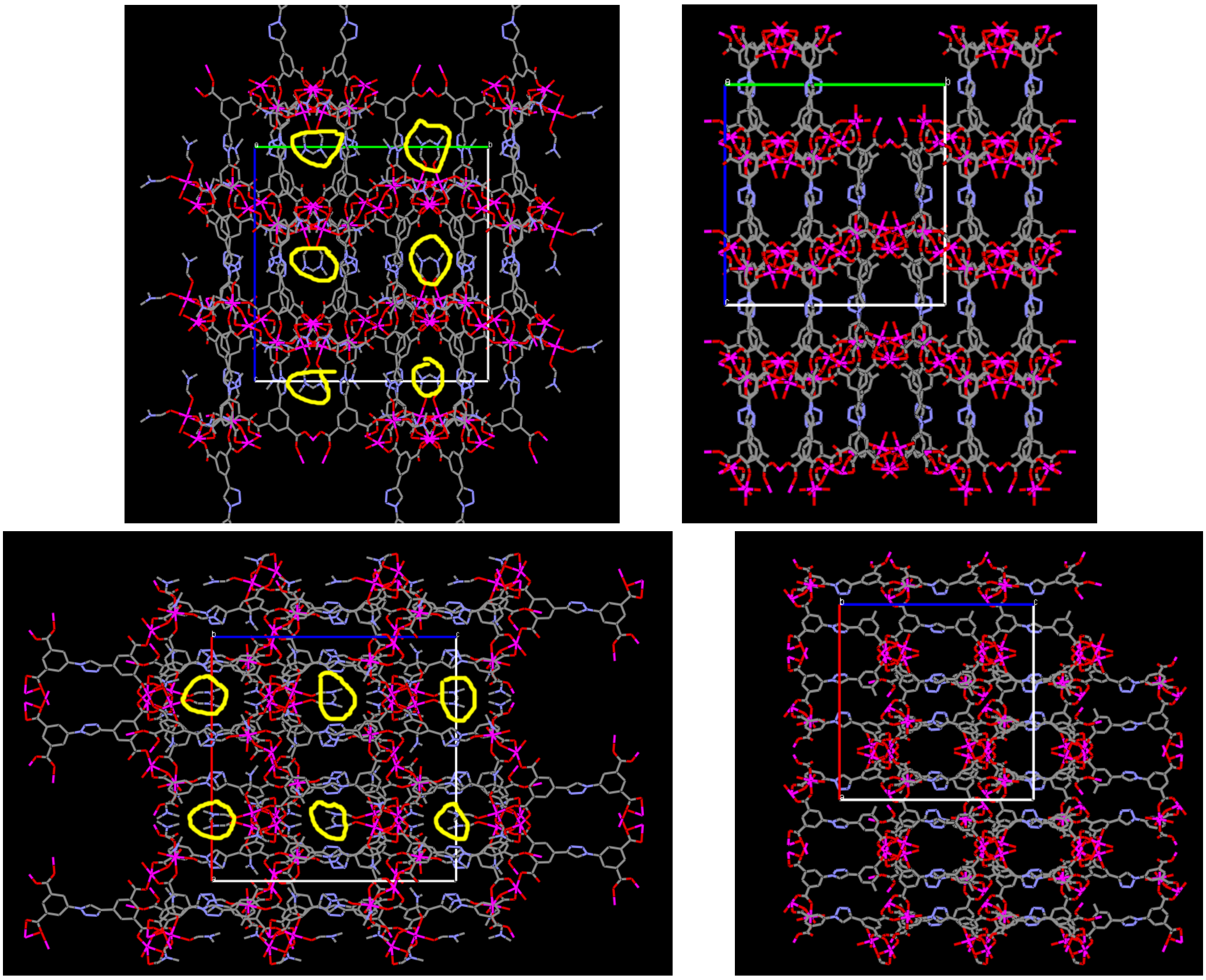

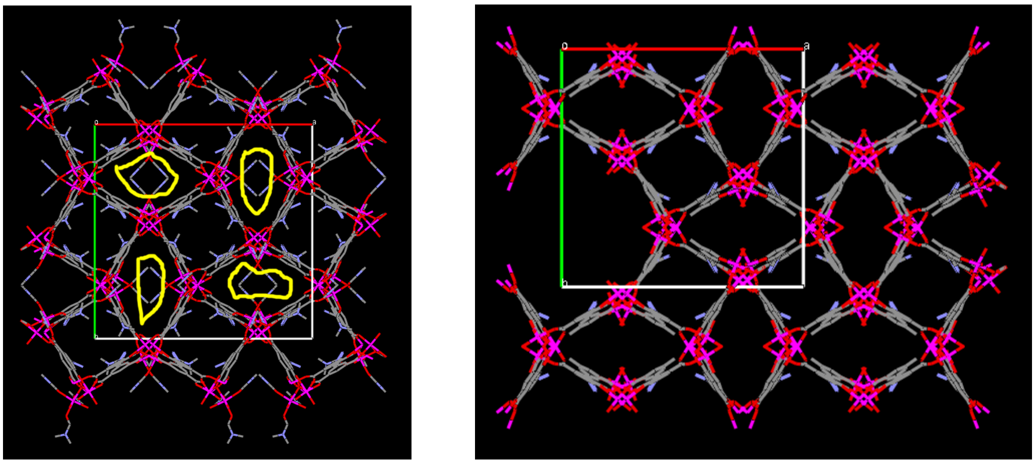

Fig. S12. The packing view of **NTU-101-Zn** along with axes *a* (top), *b* (middle), and *c* (bottom) with (left) and without (right) the coordinated DMF molecules. As shown from the left column, the coordinated DMF molecules are located in the framework channels, blocking the pores (yellow circle). Such channels would be opened upon the removal of the coordinated DMF molecules as shown from the right column. However, the removal of the coordinated DMF molecules caused the collapse of the frameworks, resulting in poor gas adsorption. Hydrogen atoms are omitted for clarity.

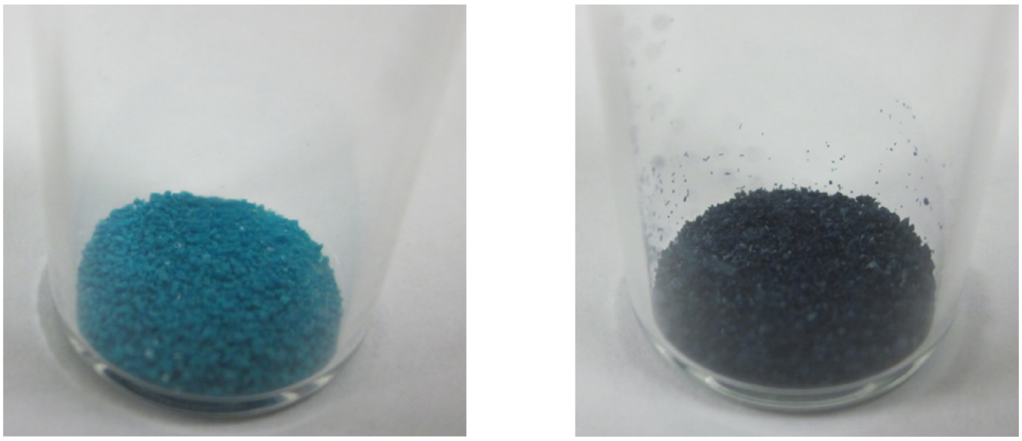

Fig. S13. Photographs of as-synthesized (left) and activated (right) **NTU-101-Cu**. The dark blue color (right) suggests the open metal sites around the Cu(II) ions and the removal of the solvent molecules. Upon exposure to air, the dark blue color returned back to its original blue color due to the adsorption of moisture.

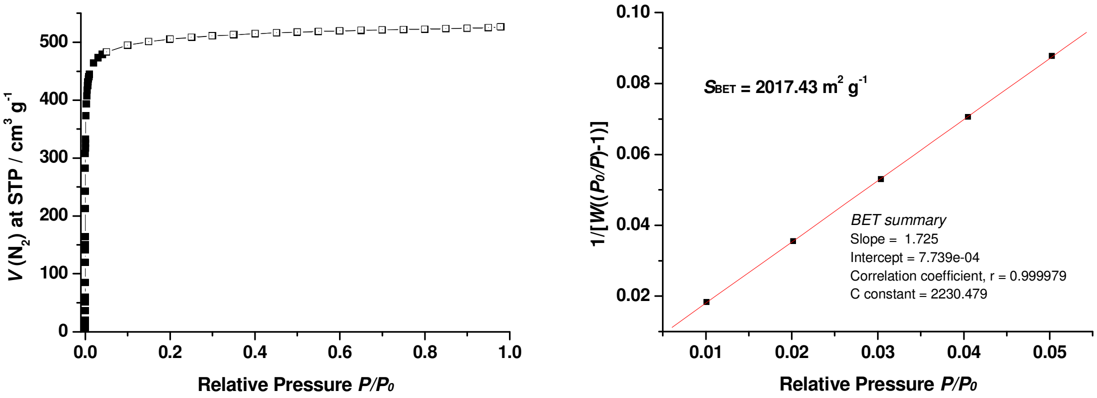

Fig. S14. Nitrogen sorption isotherm at 77K (left) and BET specific surface area plot (right) for activated **NTU-101-Cu**.

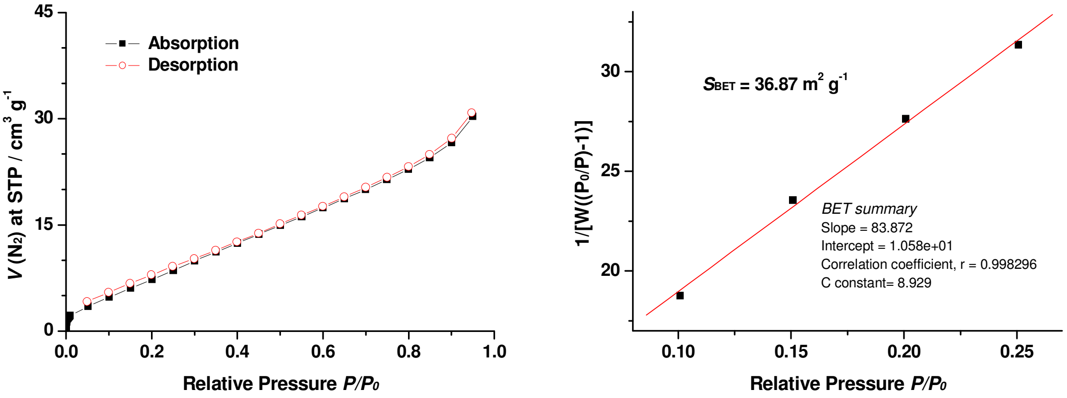

Fig. S15. Nitrogen sorption isotherm at 77K (left) and BET specific surface area plot (right) for activated **NTU-101-Zn**.

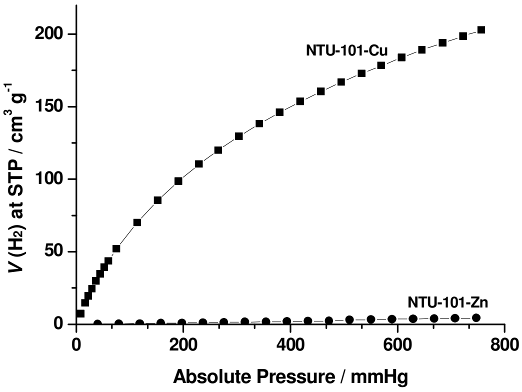

Fig. S16. H_2 adsorption isotherms of activated **NTU-101-Zn** and **NTU-101-Cu** at 77 K.

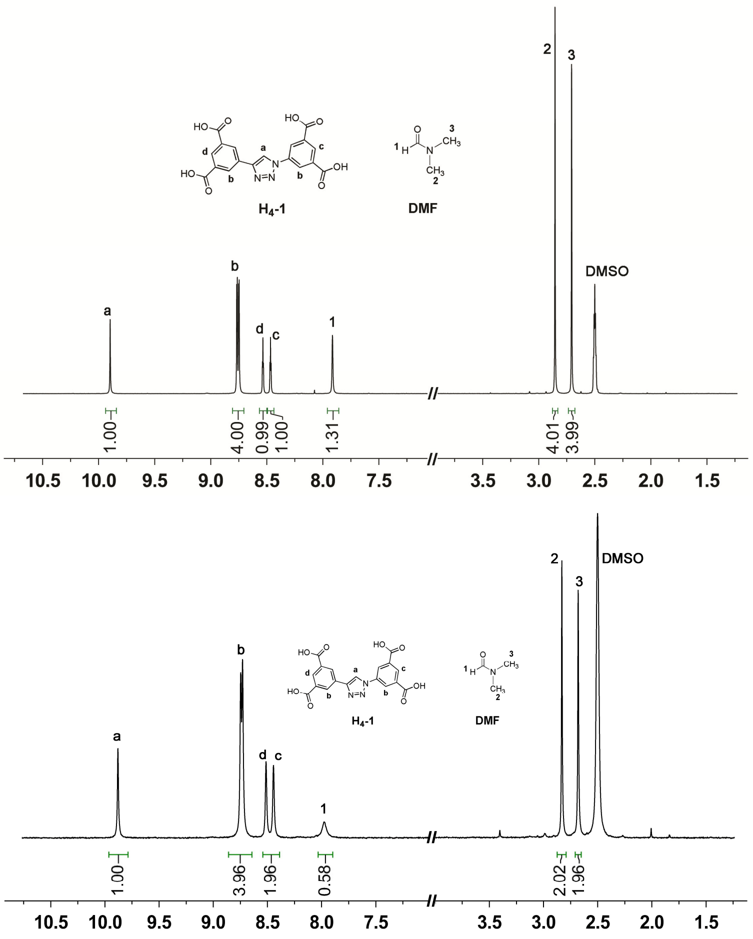

Fig. S17. ^{1}H NMR spectra of the activated **NTU-101-Zn** (top) and **NTU-101-Cu** (bottom) digested by a solution of TFA (10%) in d_6-DMSO. Less DMF molecules observed in **NTU-101-Cu** indicate the efficient removal of the coordinated DMF molecules as compared with that of **NTU-101-Zn**. The original blocked channels by the coordinated DMF molecules in **NTU-101-Zn** were opened after the Cu(II) exchange process.

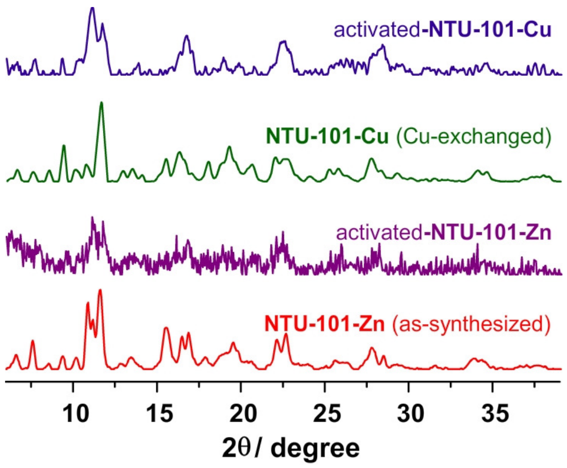

Fig. S18. Powder XRD patterns of **NTU-101-Zn** and **NTU-101-Cu** after the activation, indicating the significant collapse of the **NTU-101-Zn** framework as compared with that of **NTU-101-Cu** upon the activation.

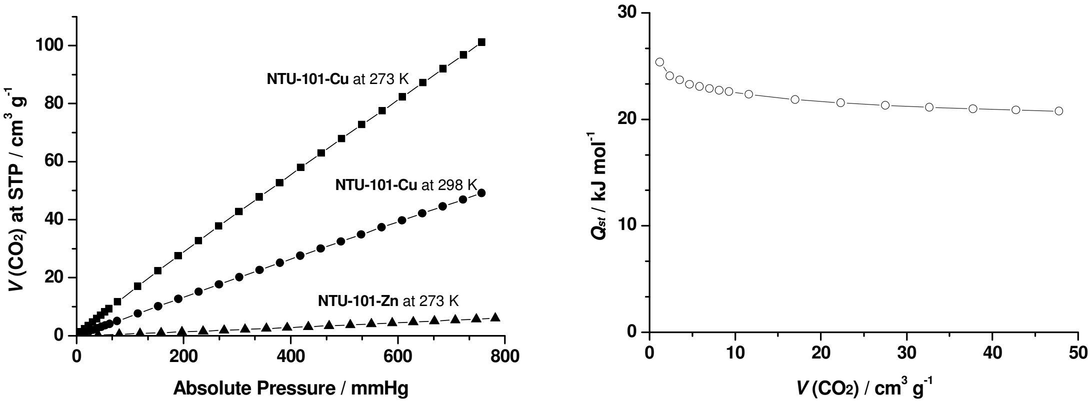

Fig. S19. CO_2 adsorption isotherms (left) of activated **NTU-101-Zn** and **NTU-101-Cu**. Isosteric heat of CO_2 adsorption (right) for activated **NTU-101-Cu** calculated from the adsorption isotherms at 273 K and 298 K.

References

S1. Z. P. Demko and K. B. Sharpless, *Angew. Chem. Int. Ed.*, 2002, **41**, 2110.

S2. G. J. Bodwell, D. O. Miller, and R. J. Vermeij, *Org. Lett.*, 2001, **3**, 2093.

S3. (a) S. Das, H. Kim and K. Kim, *J. Am. Chem. Soc.*, 2009, **131**, 3814; (b) J. Zhao, L. Mi, J. Hu, H. Hou and Y. Fan, *J. Am. Chem. Soc.*, 2008, **130**, 15222; (c) T. K. Prasad, D. H. Hong and M. P. Suh, *Chem. Eur. J.*, 2010, **16**, 14043.

S4. *SAINT V6.1*, Bruker Analytical X-ray Systems, Madison, WI, **1999**.

S5. G. M. Sheldrick, *SADABS*, Empirical Absorption Correction Program, University of Göttingen, Göttingen, Germany, **1997**.

S6. G. M. Sheldrick, *Acta Crystallogr., Sect. A: Found. Crystallogr.*, 2008, **64**, 112.

S7. A. L. Spek, *J. Appl. Crystallogr.*, 2003, **36**, 7.

Characterization spectra of key compounds

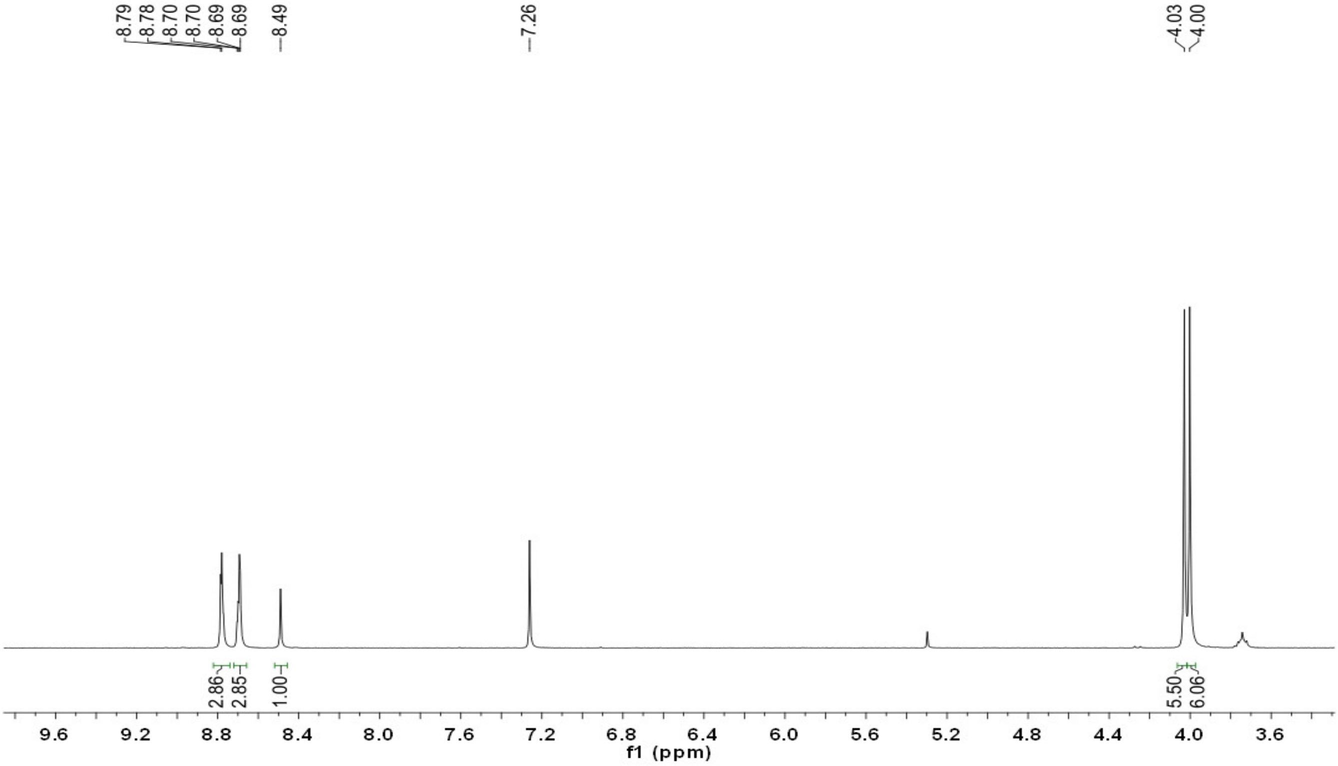

^{1}H NMR of **2** in CDCl$_3$

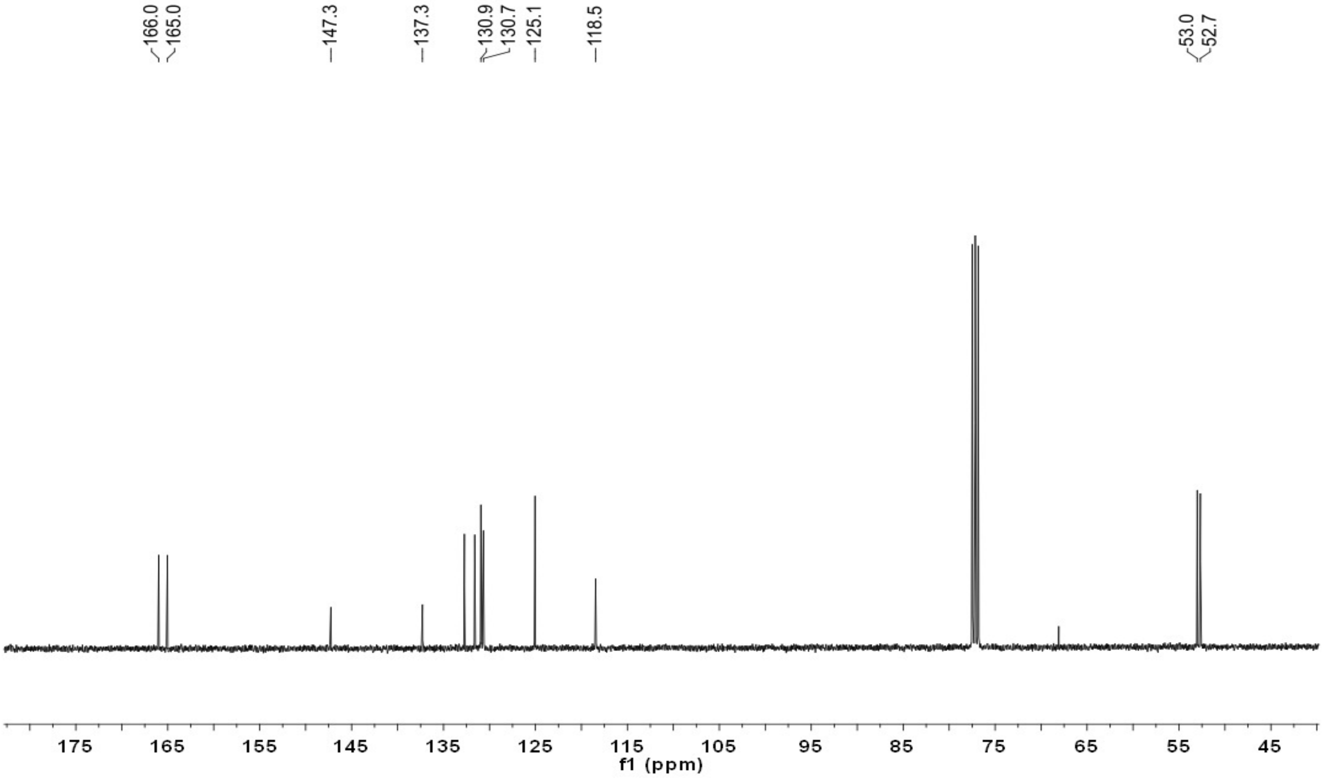

^{13}C NMR of **2** in CDCl$_3$

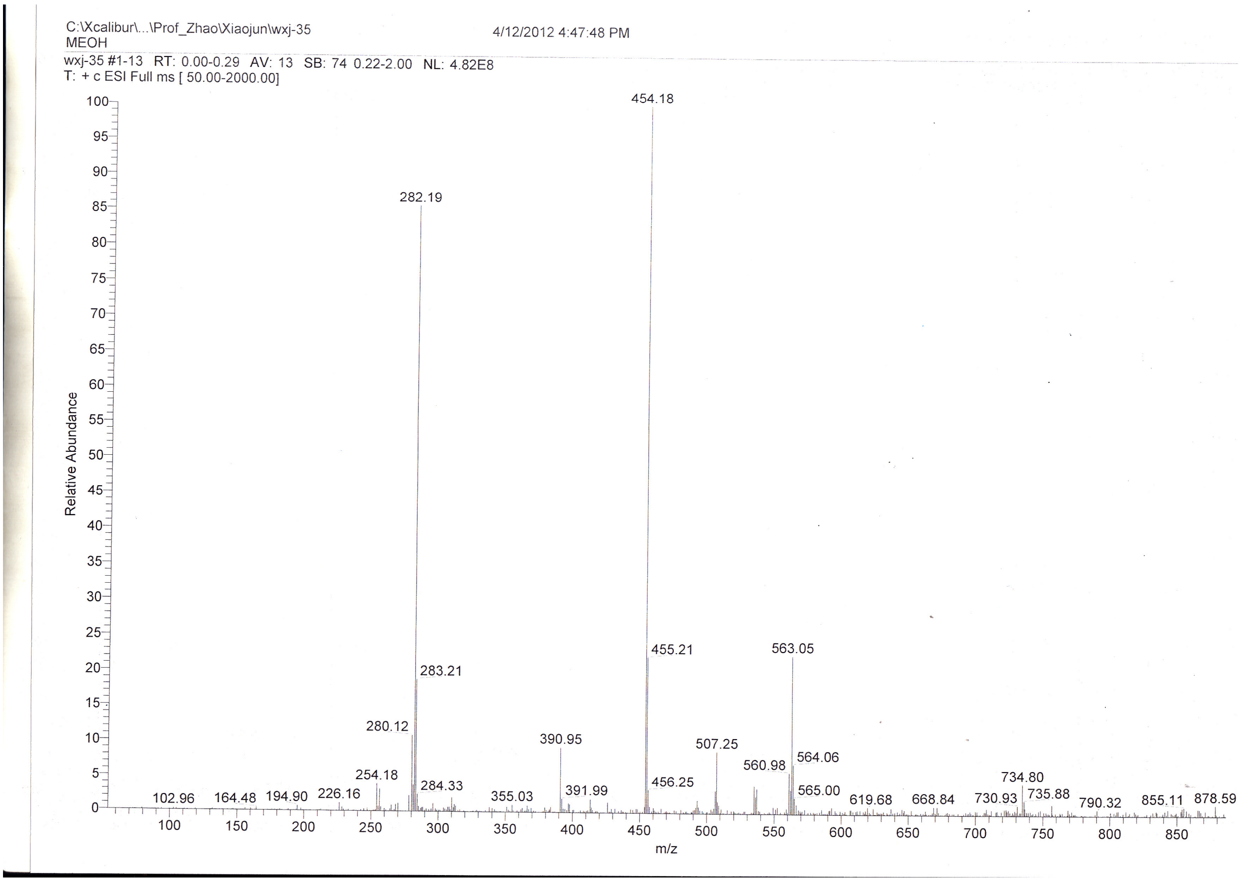

ESI-MS of **2**

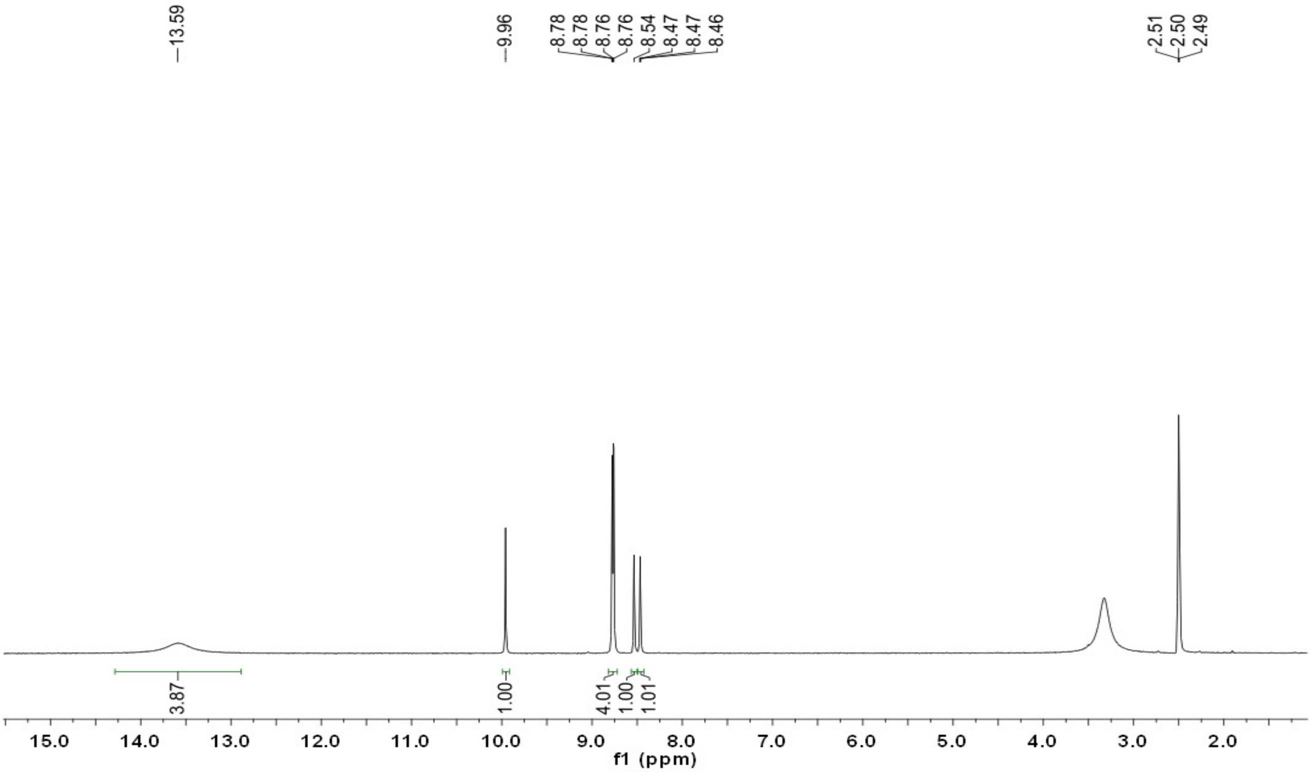

^{1}H NMR of **H_4-1** in DMSO

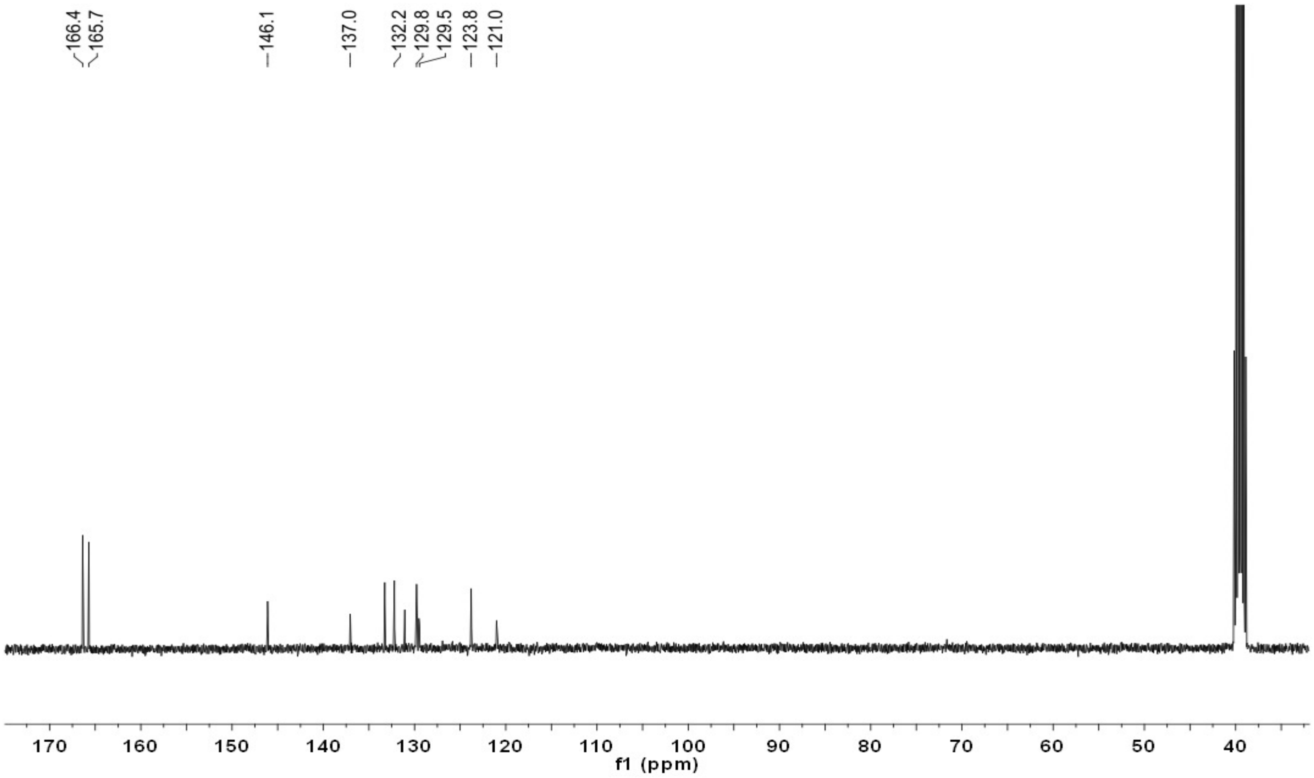

^{13}C NMR of **H_4-1** in DMSO

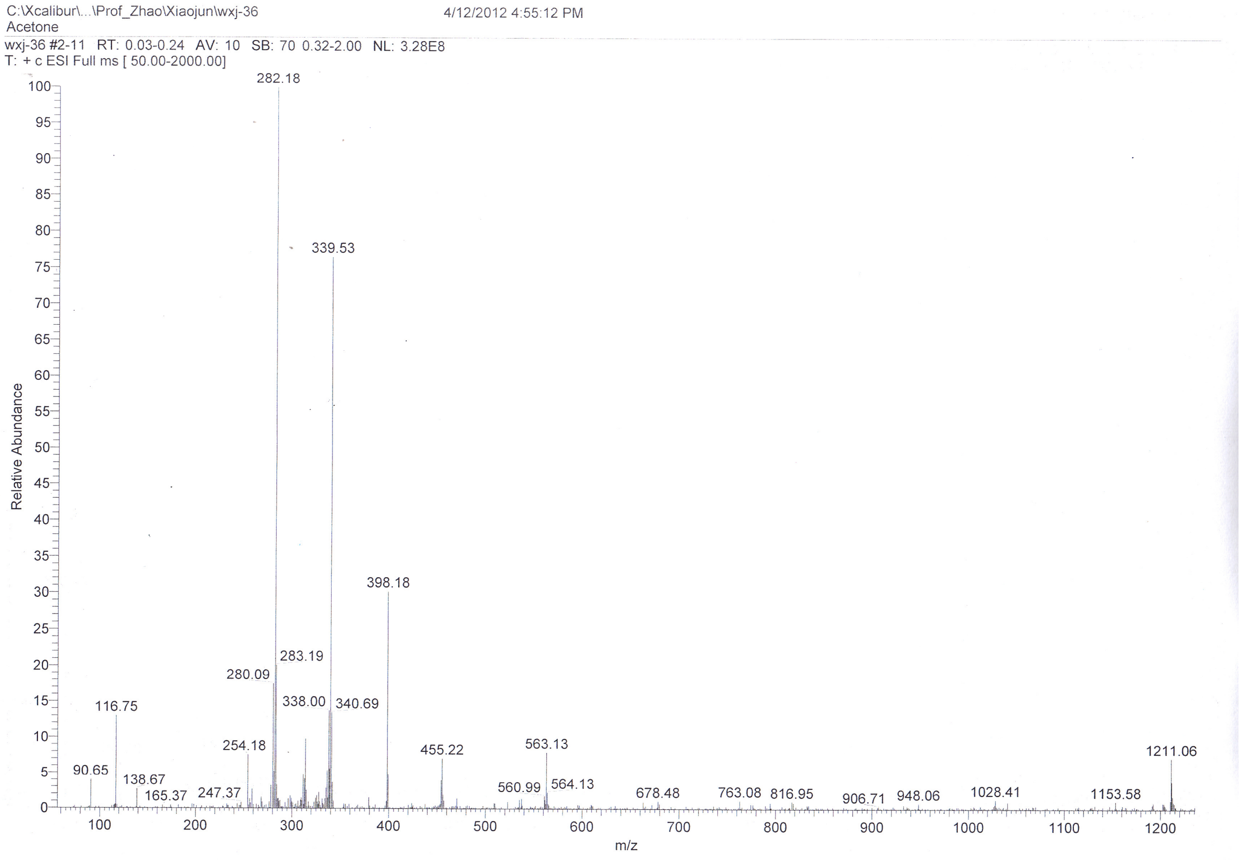

ESI-MS of **H_4-1**